Article

Nitrogen-Doped Carbon Nanotubes Supported by Macroporous Carbon as an Efficient Enzymatic Biosensing Platform for Glucose

Yonghai Song, Xingping Lu, Yi Li, Qiaohui Guo, Shuiliang Chen, Lanqun Mao, Haoqing Hou, and Li Wang

Anal. Chem., **Just Accepted Manuscript** • DOI: 10.1021/acs.analchem.5b03938 • Publication Date (Web): 10 Dec 2015

Nitrogen-Doped Carbon Nanotubes Supported by Macroporous Carbon as an Efficient Enzymatic Biosensing Platform for Glucose

Yonghai Song[†], Xingping Lu[†], Yi Li[†], Qiaohui Guo[†], Shuiliang Chen[†], Lanqun Mao[‡], Haoqing Hou[†] and Li Wang[†,*]

[†]*Key Laboratory of Functional Small Organic Molecule, Ministry of Education, Key Laboratory of Chemical Biology, Jiangxi Province, College of Chemistry and Chemical Engineering, Jiangxi Normal University, Nanchang 330022, China.*

[‡]*Beijing National Laboratory for Molecular Sciences, Key Laboratory of Analytical Chemistry for Living Biosystems, Institute of Chemistry, Chinese Academy of Sciences, Beijing 100190, China.*

∗Corresponding author: Tel/Fax: +86 791 88120861. E-mail: lwangsy2003@hotmail.com (L. Wang).

ABSTRACT

Effective immobilization of enzymes/proteins on electrode surface is very essential for biosensor development, but it still remains challenging because enzymes/proteins tend to form close-packed structures on electrode surface. In this work, nitrogen-doped carbon nanotubes (NCNTs) supported by three-dimensional Kenaf Stem-derived porous carbon (3D-KSC) (denoted as 3D-KSC/NCNTs) nanocomposites were constructed as the supporting matrix to load glucose oxidase (GOD) for preparing integrated glucose biosensors. These NCNTs are vertically arrayed on the channel walls of the 3D-KSC via chemical vapor deposition method, which could noticeably increase the effective surface area, mechanical stability and active sites (originated from the doped nitrogen) of the nanocomposites. The integrated glucose biosensor exhibits some advantages over the traditional GOD electrodes in terms of the capability to promote the direct electron transfer of GOD, enhance the mechanical stability of the biosensor attributed to the strong interaction between NCNTs and GOD, and enlarge the specific surface area to efficiently load a large number of GOD. The as-prepared biosensor shows a good performance toward both the oxygen reduction and the glucose biosensing. This study essentially offers a novel approach for the development of biosensors with excellent analytical properties.

INTRODUCTION

Carbon nanotubes (CNTs) have been widely developed as supports to immobilize enzymes/proteins (e.g. glucose oxidase (GOD), horseradish peroxidase (HRP), acetylcholinesterase (AChE)) for biosensors because they can promote the direct electron transfer (DET) between the redox active sites of enzymes/proteins and the electrodes effectively, thus improve the sensitivity of biosensors accordingly.[1-4] For example, a sensitive glucose biosensor based on GOD layer-by-layer self-assembled on CNTs was reported.[3] However, there still exists a problem in the mechanical stability for the enzyme electrodes prepared by casting the CNTs on the electrode surfaces directly, which limit their practical applications. Furthermore, it is very hard to disperse the CNTs on the electrode surfaces uniformly, which is expected to be unfavorable for the DET of enzymes/proteins. Moreover, CNTs tend to form close-packed structures, resulting in the difficulties in maintaining the large surface areas of CNTs and the mass transfer within the CNT networks. Hence, CNTs are proposed loading on graphene or carbon cloth to form composites for enhancing the usage of CNTs and reducing the aggregation.[5-8]

On the other hand, nanomaterials with three-dimensional (3D) hierarchical nanostructures, such as self-supported array structures, flower-like structures and layered structures, have been introduced as support or catalyst to improve electrochemical performance.[9-13] For example, free-standing NiO nanoflake arrays were used for nonenzymatic glucose sensor with a high sensitivity of 8500 μA cm^{-2} mM^{-1} and a low detection limit of 1.2 μM.[14] A CuO flower-like nanostructured sensor for nonenzymatic H_2O_2 detection was obtained through the chemical oxidation of copper foil showing a sensitivity of 88.4 μA cm^{-2} mM^{-1} and a wide linear range from 42.5 μM to 40 mM.[12] Generally, these nanomaterials with 3D hierarchical nanostructures have large specific surface area and could been directly used as catalyst to construct nonenzymatic sensors.

However, their large size would cause the structural instability or easy to fall off from the electrode surface, resulting in the instable performance.

Recently, our group developed a kind of Kenaf Stem-based porous carbon (3D-KSC) integrated electrodes, which were successfully used as the supporting matrix to load nanostructures or biomolecules as sensing platforms.[15] The 3D-KSC-derived materials could provide ultrahigh specific surface area for the effective immobilization of plenty of electroactive materials. Some microporosities and defects of the integrated 3D-KSC electrodes promote the immobilization of electroactive materials greatly. Both the 3D hierarchically porous nanostructures and the good electrical conductivity enhance the mass and electron transfer together. Unfortunately, macropores of dozens of micrometers in the 3D-KSC might prevent them from further applications in biosensors.

In this work, nitrogen-doped CNTs (NCNTs) supported by 3D-KSC (denoted as 3D-KSC/NCNTs) nanocomposites were developed as a novel enzymatic biosensing platform for the detection of glucose. The NCNTs networks are densely arrayed on the channel walls of the 3D-KSC via the C-C bond, which enhances the stability of 3D-KSC/NCNTs nanocomposites greatly and increases both the effective surface area and active sites. The 3D-KSC/NCNTs nanocomposites show good catalytic properties for oxygen reduction reaction (ORR) owing to the excellent structure and NCNTs. Then, the 3D-KSC/NCNTs nanocomposites were further employed to load GOD based on the strong interaction between NCNTs and GOD for glucose biosensing, exhibiting good electrochemical performance.

■ EXPERIMENTAL SECTION

Chemicals and Reagents. GOD (140 U mg^{-1}) was purchased from Sigma–Aldrich. Graphite powder (spectrum pure), glucose, nickel acetate ($Ni(CH_3COO)_2 \cdot 4H_2O$), uric acid (UA), ascorbic

acid (AA), dopamine (DA), fructose, galactose, sucrose and mannose were purchased from Sinopharm Chemical Reagent Co., Ltd (Shanghai, China). The Kenaf Stem (KS) was provided by Futian farm (Ji'an, China). Phosphate buffer solution (PBS) was obtained by mixing 0.2 M NaH_2PO_4 and Na_2HPO_4. The GOD solution (10 mg mL^{-1}) was prepared in 0.2 M PBS (pH 7.0) and stored at 4 °C. All reagents were used without further purification. All solutions were prepared with ultra-pure water, purified by a Millipore-Q System (18.2 MΩ cm).

Preparation of the 3D-KSC/NCNTs Nanocomposites. The 3D-KSC was obtained by carbonizing dried KS directly.[15] The carbonization was performed in a tubular quartz reactor under N_2 atmosphere with a ramp of 5 ºC min^{-1} and annealed at 700 ºC for 2 h. To prepare the 3D-KSC/NCNTs nanocomposites, the dried KS was firstly immersed in a nickel acetate aqueous solution (20 mM) for about 15 days. After drying at 80 ºC, the soaked KS was carbonized in a tubular quartz reactor under N_2 atmosphere with a heating rate of 5 ºC min^{-1} and annealed at 700 ºC for 2 h to obtain the 3D-KSC/Ni nanoparticles (NPs). Then, the 3D-KSC/Ni NPs were annealed at 700 ºC for 1 h under H_2/pyridine atmosphere to allow the growth of NCNTs. The pyridine was injected into the quartz tube (0.1 mL min^{-1}) via a syringe loaded into the syringe pump.[16] The procedure is shown in Scheme 1.

Preparation of the Integrated 3D-KSC/NCNTs and 3D-KSC/NCNTs/GOD Electrode. The integrated 3D-KSC/NCNTs electrode was prepared similar to our previous work.[15] The integrated 3D-KSC/NCNTs/GOD electrode was obtained by further immersing the 3D-KSC/NCNTs electrode into 10 mg mL^{-1} GOD solution for 2 days, then dried and stored at 4 ºC for further use. The preparation procedure and the corresponding discussion are also illustrated in Figure S1 (Supporting Information).

Instruments. Scanning electron microscopy (SEM) images were obtained using a HITACHI

S-3400N scanning electron microscope at an accelerating voltage of 15 kV. Fourier transform infrared spectroscopy (FT-IR) was recorded on a Perkin–Elmer Spectrome 100 spectrometer (Perkin–Elmer Company, USA) using KBr pellets. N_2 adsorption/desorption isotherms were measured at -196 ℃ using an ASAP 2020 instrument (Micromeritics). Before the experiments, the samples were degassed under vacuum at 120 ℃. Raman spectra were performed at room temperature with a LabRAM HR spectrometer and an argon ion laser operating at a wavelength of 632.8 nm as the excitation (Jobin Yvon Ltd, France). X-ray photoelectron spectroscopy (XPS) measurements were performed on an ESCALAB-MKII spectrometer (VGCo., United Kingdom) with Al Kα X-ray radiation as the X-ray source for excitation.

Cyclic voltammograms (CVs) were performed in a quiescent solution on a CHI 660C electrochemical workstation (Shanghai, China) at room temperature. A conventional three-electrode system was adopted including a platinum wire as the counter electrode, an Ag/AgCl (saturated KCl) or a saturated calomel electrode (SCE) as the reference electrode and the 3D-KSC/NCNTs or 3D-KSC/NCNTs/GOD electrode as the working electrode. Electrochemical impedance spectroscopy (EIS) was characterized at open circuit potential in the frequency range from 10^4 Hz to 0.01 Hz with a signal amplitude of 5 mV. Rotating disk electrode (RDE) measurements were performed in O_2-saturated 0.1 M KOH solution with rotation rates from 400 to 2500 rpm at 10 mV s^{-1} using a glassy carbon disk electrode (Pine Instruments, 5.0 mm in diameter, A=0.19625 cm^2) as the working electrode, a Pt plate as the counter electrode and an Ag/AgCl (saturated KCl) as the reference electrode.

■ RESULTS AND DISCUSSION

Characterization of the 3D-KSC/NCNTs Nanocomposites. The morphologies of 3D-KSC/NCNTs nanocomposites were examined by SEM. As shown in Figure 1A, the 3D-KSC

has hollow structure inside. The high-magnification images of the top view (Figure 1B) and the side view (Figure 1D) show 3D macroporous structure with dozens of micrometers.[15] Figure 1C, E and F show the top view, side view and cross-section view of 3D-KSC/NCNTs, respectively. The NCNTs are observed to be densely distributed on the channel walls which rough the channel walls greatly. The high-magnification images (insets in Figure 1C, E and F) clearly show that these NCNTs are almost vertically grown on the channel walls of 3D-KSC.

More detailed information can be obtained from further magnified SEM images of the 3D-KSC/NCNTs (Figure S2, Supporting Information). As can be seen from the top view (Figure S2A, Supporting Information), side view (Figure S2B, Supporting Information) or cross-section view (Figure S2C, Supporting Information), the NCNTs form a mesh structure by themselves and array well on the channel walls of the 3D-KSC. The cross-section view indicates the amount of NCNTs inside is less than that distributed on the surface because it is more difficult for the H_2/pyridine gas mixture to go into the interior of 3D-KSC. The high-magnification images (Figure S2D, E and F, Supporting Information) show some Ni NPs loaded on the end of the NCNTs, which are used as catalyst for the growth of NCNTs. As a control, the formation of 3D-KSC/Ni NPs was also investigated by SEM (Figure S3, Supporting Information). Obviously, as shown in the top view (Figure S3A, Supporting Information), side view (Figure S3B, Supporting Information) or cross-section view (Figure S3C, Supporting Information), a lot of Ni NPs are formed on the surface of 3D-KSC. The high-magnification images (Figure S3D−F, Supporting Information) show the Ni NPs distribute on the channel walls uniformly, and only a few aggregates and larger NPs are found, which provide sufficient catalysts for the growth of NCNTs. Besides that, the growth time is also very important for the growth of NCNTs. The SEM images of 3D-KSC/NCNTs obtained with the growth time of 20 min are recorded in Figure S4 (Supporting Information). It can be observed that

only a small number of NCNTs were formed. Therefore, enough reaction time is necessary to form a large number of NCNTs.

"Here Figure 1"

FT-IR spectroscopy was further used to characterize the 3D-KSC/NCNTs nanocomposites (Figure 2A). For 3D-KSC (black line), the peaks at 3440, 1571 and 1216 cm^{-1} are corresponding to –OH, C=C, and C-C stretching vibration, respectively.[17,18] After chemical vapor deposition (CVD) (red line), the appearance of the peak at 1300 cm^{-1} corresponding to the vibration of C-N indicates the formation of NCNTs.[19,20] N_2 adsorption/desorption isotherm (as shown in Figure 2B) was used to determine the surface area of 3D-KSC/NCNTs nanocomposites showing a very high BET surface area of 1855 m^2 g^{-1} (red line), which is about 1.8 times as that of the blank 3D-KSC (1030 m^2 g^{-1}, black line). Raman spectra (Figure 2C) of both 3D-KSC (black line) and 3D-KSC/NCNTs (red line) display D band and G band at about 1330 and 1576 cm^{-1}, respectively. The relatively higher peak intensity ratio of D/G band of 3D-KSC/NCNTs (I_D/I_G=1.75) than that of 3D-KSC (I_D/I_G=1.52) is obtained, indicating the presence of a large number of structure defects after the introduction of NCNTs because the N atoms are introduced into the carbon lattice,[21,22] which is beneficial for the electrocatalysis of ORR as defects to provide active sites in the electrocatalytic reactions.[23] In addition, XPS spectrum was employed to confirm the elemental surface composition of the 3D-KSC/NCNTs nanocomposites, and the results are shown in Figure 2D. The XPS spectrum of 3D-KSC/NCNTs (red line) possesses C 1s (282.5 eV), N 1s (398.1 eV) and O 1s (528.6 eV) peaks, while 3D-KSC (black line) only has C 1s (282.5 eV) and O 1s (528.6 eV) peaks. The N 1s peak verifies the existence of N element in the 3D-KSC/NCNTs nanocomposites. The atomic percentage of N is calculated to be about 3.96 %. The inset in Figure 2D displays detailed spectra of N 1s, three peaks at 397.7, 399.5 and 401.2 eV could be seen, corresponding to the pyridinic-N, pyrrolic-N and

graphitic-N, respectively.[24-27] In addition to benefiting for the electrocatalysis of ORR, the N atoms in CNTs brought in defect structure can also be acted as the active sites for GOD adsorption.

"Here Figure 2"

The electron transfer behavior of the integrated 3D-KSC/NCNTs electrode was evaluated with CVs using the probe of 5.0 mM $K_3Fe(CN)_6$ in 0.1 M KCl solution under scanning rate of 50 mV s^{-1} (Figure S5A, Supporting Information). The peak current increased significantly at the integrated 3D-KSC/NCNTs electrode as compared with the 3D-KSC electrode and GCE because the NCNTs loaded on the 3D-KSC enlarged its specific surface area greatly. Furthermore, the peak-to-peak potential separation of 3D-KSC/NCNTs electrode is close to that of 3D-KSC electrode and GCE, indicating the arrayed NCNTs have no obvious influence on the electron transfer of the 3D-KSC/NCNTs electrode due to the excellent electrical conductivity of NCNTs and porous arrayed structures. The working potential window of the 3D-KSC/NCNTs electrode was estimated to be about 2.9 V with 0.1 M pH 7.0 PBS (Figure S5B, Supporting Information), which is similar to that of GCE (3.3 V) and wider than that of the 3D-KSC electrode (2.6 V).

ORR Performance of the 3D-KSC/NCNTs Nanocomposites. Owing to their excellent properties, the 3D-KSC/NCNTs nanocomposites might be extensively applied in a variety of fields. First of all, the 3D-KSC/NCNTs can be directly used as a catalyst for ORR. As we know, the cathodic ORR is very crucial for the performance of fuel cells.[28] Developing effective ORR electrocatalysts has been the focus of commercialization of fuel cells. Furthermore, most enzymatic glucose biosensors detect the concentration of glucose by monitoring the mount of O_2, which could be measured in ORR. Thus, the electrocatalytic activity of the 3D-KSC/NCNTs for ORR was firstly investigated by CVs for further application in glucose biosensing (Figure 3A). A reduction peak for ORR about −0.40 V appears at the 3D-KSC/NCNTs electrode (red line), but there is no obvious

reduction peak for ORR at the 3D-KSC electrode (black line), which indicates a much higher catalytic activity and improved electron transfer kinetics of 3D-KSC/NCNTs for ORR. Figure 3B give the CVs of the 3D-KSC/NCNTs nanocomposite electrode in 0.1 M KOH solution under N_2-saturated (black line), air-saturated (red line) and O_2-saturated (green line) conditions, respectively. The CVs shows an unconspicuous peak in N_2-saturated KOH solution, appears an obvious ORR peak in air-saturated KOH solution, while exhibits a significantly increased ORR peak in O_2-saturated KOH solution.

To further explain the electron transfer process of the 3D-KSC/NCNTs nanocomposites during the ORR, RDE was employed to follow the reaction kinetics. The linear sweep voltammograms of the 3D-KSC/NCNTs in O_2-saturated 0.1 M KOH with rotation rates varying from 400~2500 rpm at 10 mV s^{-1} are recorded in Figure 3C. The current density increases with the increased rotation rate. The number of electron transfer (n) in the ORR could be calculated based on Koutecky–Levich equations [Eqs. (1)–(2)]:[28-31]

$$j^{-1} = j_k^{-1} + \left(B\omega^{1/2}\right)^{-1} \quad (1)$$

$$B = 0.62nFCD^{2/3}\nu^{-1/6} \quad (2)$$

where j is the determined current density, j_k is the kinetic-limiting current density, ω is the angular velocity of rotation ($\omega = 2\pi N$, here N is the linear rotation speed), n is the overall number of electron transfer during ORR, F is the Faraday constant (96485 C mol^{-1}), C is the bulk concentration of O_2 (1.2×10^{-6} mol cm^{-3}), D is the O_2 diffusion coefficient (1.9×10^{-5} cm^2 s^{-1}), and ν is the kinetic viscosity of 0.1 M KOH (0.01 cm^2 s^{-1}). The corresponding Koutecky–Levich plots (j^{-1} vs $\omega^{-1/2}$) at potentials varied from −0.30 to −0.60 V exhibits good linearity (Figure 3D). The dependence of n on the potential is shown as an inset in Figure 3D. The n value is about 3.5-3.8 at potential range of −0.30 to −0.60 V, suggesting that ORR at the KSC/NCNTs mainly involves a

four-electron transfer pathway.

"Here Figure 3"

In addition, the stability of 3D-KSC/NCNTs nanocomposites in ORR is also tested by CVs (Figure S6A, Supporting Information) and current–time curve (Figure S6B, Supporting Information) in the O_2-saturated 0.1 M KOH solution. The maximum ORR current density is almost invariable after 1000 cycles in the CVs. And the 3D-KSC/NCNTs electrode exhibits an excellent durability at –0.40 V in the current–time curve with only about 5.43 % decrease in current density after 8000 s. The results indicate that the 3D-KSC/NCNTs nanocomposites have long-term stability for ORR.

Glucose Biosensing at the 3D-KSC/NCNTs/GOD Electrode. Considering GOD could catalyze the oxidation process of glucose into gluconolactone companying by the reduction of oxygen, thus glucose could be quantitatively detected by sensing the amount of oxygen consumed in the reduction.[32-34] That is, we could also detect glucose by the decrease of the cathodic peak current in ORR. Therefore, the 3D-KSC/NCNTs nanocomposites are further applied for glucose biosensing via the immobilization of GOD. EIS was firstly used to study the charge transfer and ion diffusion process of the 3D-KSC/NCNTs/GOD electrode (Figure S7, Supporting Information). The resistance of charge transfer (R_{ct}) of the 3D-KSC/NCNTs/GOD electrode (389 Ω) is much smaller than that of the 3D-KSC/GOD electrode (994 Ω), which indicates the KSC/NCNTs could improve the charge transfer and ion diffusion significantly. The DET of GOD on the 3D-KSC/NCNTs/GOD electrode was studied by CVs. Figure 4A show typical CVs of the 3D-KSC/GOD (red line) and the 3D-KSC/NCNTs/GOD (black line) in N_2-saturated PBS (0.2 M, pH 7.0) at a scan rate of 100 mV s^{-1}. At the 3D-KSC/GOD electrode (red line), a pair of weak redox peaks appears. While, the 3D-KSC/NCNTs/GOD electrode (black line) shows a pair of well-defined redox peaks with anodic (E_{pa}) and cathodic (E_{pc}) peak potentials of −0.354 V and −0.403 V, respectively, which are

attributed to the FAD/$FADH_2$ redox couples in GOD.[35-37] The peak-to-peak separation ($\Delta E_p=E_{pa}-E_{pc}$) is around 49 mV, indicating a fast DET of GOD. These results indicate that the NCNTs could enhance the DET between the redox active sites of GOD and the electrode owing to the strong interaction between NCNTs and GOD, the effective loading of GOD and their excellent electrical conductivity together.

CVs of the 3D-KSC/NCNTs/GOD electrode in N_2-saturated PBS solution (0.2 M, the pH varied from 6.0 to 8.0) at a scan rate of 100 mV s^{-1} are shown in Figure 4B. The redox peak potential negatively shifts with the increasing of pH. The formal potential ($E^0 = (E_{pa} + E_{pc})/2$) exhibits a linear dependence over different pH with a slope of −52 mV/pH (inset in Figure 4B). The value is close to the theoretical value (−58.6 mV/pH) of FAD/$FADH_2$ redox couples possessing a two-electron and two-proton transportation process. The possible mechanism could be expressed as following [Eqs. (3)−(4)]:[37-40]

$$\text{Glucose} + \text{GOD(FAD)} + 2e^- + 2H^+ \leftrightarrow \text{Gluconolactone} + \text{GOD}(FADH_2) \quad (3)$$

$$\text{GOD}(FADH_2) + O_2 \rightarrow \text{GOD(FAD)} + H_2O_2 \quad (4)$$

The CVs of 3D-KSC/NCNTs/GOD electrode at varied scan rates is also recorded in Figure 4C. The peak current increases linearly with the increasing scan rate from 100 to 1000 mV s^{-1} (inset in Figure 4C), which suggests the electron transfer reaction results from a surface-controlled process. At the scan rate of 100 mV s^{-1}, with ΔE_p=49 mV and $n\Delta E_p$<200 mV, the electron transfer coefficient (α) is estimated to be 0.5. The electron-transfer rate constant (k_s) can be estimated according to Laviron theory [Eqs. (5)]:[36,41]

$$k_s = \frac{mnF\nu}{RT} \quad (5)$$

where m is a constant related to ΔE_p (here m=0.26), n is the electron transfer number (here n=2), F is the Faraday constant (96485 C mol^{-1}), ν is the scan rate (0.1 V s^{-1}), R is the gas constant (8.314 J

mol^{-1} K^{-1}), and T is the temperature in Kelvin (298 K). The value of k_s is estimated to be 2.03 s^{-1} for the 3D-KSC/NCNTs/GOD, which is higher than that of the 3D-KSC/GOD (1.93 s^{-1}). The k_s is also much larger than that of gelatin-multiwalled carbon nanotube/GOD/glutaraldehyde/GCE (1.08 s^{-1})[35] and CNTs/AuNPs/PDDA-GOD/GCE (1.01 s^{-1})[42] reported previously. The result further indicates that the NCNTs do promote the DET of GOD.

The CVs of 3D-KSC/NCNTs/GOD electrode in O_2-saturated PBS (0.2 M, pH 7.0) at scan rate of 100 mV s^{-1} with different glucose concentration is shown in Figure 4D. The cathodic current decreases linearly with the increasing glucose concentration in the range of 5.8 μM−18.0 mM (R=0.9942) with a detection limit of 1.93 μM and a sensitivity of 29.4 μA mM^{-1} cm^{-2} (Inset in Figure 4D). The linear range of 3D-KSC/NCNTs/GOD is much wider than that of KSC/GOD (11.2 μM−12.0 mM) and previous GOD biosensor including GOD on the Ag-polydopamine@CNTs nanocomposite (0.05–1.1 mM),[40] GOD adsorbed into a nanoporous TiO_2 film layered on the surface of an iron phthalocyanine vertically aligned CNTs modified electrode (0.05–4.0 mM),[4] GOD at a Mn-doped ZnS quantum dots modified electrode (0.01–0.1 and 0.1–1.0 mM),[43] and GOD immobilized on polyvinyl alcohol and partially prehydrolyzed tetraethyl orthosilicate modified electrode (1.0–8.0 mM).[44] The more detailed comparison between the 3D-KSC/NCNTs/GOD and other GOD-based glucose sensors is listed in Table S1 (Supporting Information). By comparing, the 3D-KSC/NCNTs/GOD biosensor offers a reasonable sensitivity, a low detection limit and the widest linear range. Such good performance may be attributed to the fact that the NCNTs are densely arrayed on the channel walls via the C-C bond, which greatly increase the effective surface area, mechanical stability and active sites. Moreover, the 3D-KSC/NCNTs nanocomposites are used as supports to immobilize GOD effectively, which overcome some disadvantages of traditional GOD electrodes, such as difficult DET of GOD, mechanical instability and stacking of supports,

and negative influence of dispersants. Therefore, the 3D-KSC/NCNTs/GOD electrode exhibits an excellent sensing performance, indicating a potential practical application in the future.

"Here Figure 4"

The stability of the 3D-KSC/NCNTs/GOD biosensor was investigated and the result is shown in Figure S8A (Supporting Information). After 15 days, the catalytic current response of 2.0 mM glucose only decreases by 3.5 %, demonstrating a good stability. To evaluate the electrode-to-electrode reproducibility, six 3D-KSC/NCNTs/GOD sensors were prepared in the same way. The responses of the six sensors toward 2.0 mM glucose show a RSD of 3.4 % (Figure S8B, Supporting Information). The selectivity of 3D-KSC/NCNTs/GOD biosensor was also studied. Figure S9 (Supporting Information) presents the catalytic current response of the sensor to 2.0 mM glucose including 10-fold concentration of interfering substances such as some sugars, UA, AA and DA. No obvious interference is observed because GOD exhibits maximum activity at the optimal pH and can specially recognize the glucose accordingly. Furthermore, the 3D-KSC/NCNTs nanocomposites provide a good biocompatible environment to keep the bioactivity of GOD on electrode surface. The good selectivity, stability and reproducibility of the 3D-KSC/NCNTs/GOD make it a promising material for glucose biosensor. The detection of glucose in blood serum samples indicates the biosensor to perform very well (Table S2, Supporting Information). Figure S10 (Supporting Information) shows the stability of 3D-KSC/NCNTs/GOD in the determination of glucose for blood serum sample. 94.4 % of the initial response is retained for the biosensor after storing in the refrigerator at 4 ºC over 15 days. The results indicate that the 3D-KSC/NCNTs/GOD electrode is stable enough to be potentially used to detect glucose selectively in a practical sample.

■ CONCLUSIONS

In conclusion, the 3D-KSC/NCNTs nanocomposites were constructed by growing NCNTs on the

3D-KSC directly by a simple CVD method. The NCNTs are densely arrayed on the channel walls of the 3D-KSC via the C-C bond, which could increase the effective surface area, mechanical stability and active sites greatly. Both the construction and the NCNTs contribute to the good catalytic performance of the 3D-KSC/NCNTs nanocomposites for ORR, which is necessary for the quantitative detection of glucose by monitoring the amount of oxygen consumed in the reduction reaction. Moreover, the 3D-KSC/NCNTs nanocomposites can be used as a supporting matrix to immobilize GOD through the strong interaction between NCNTs and GOD for glucose biosensing. The 3D-KSC/NCNTs/GOD electrode shows effective DET and wide linear range for glucose detection because it overcome some disadvantages of traditional GOD electrodes, such as difficult DET of GOD, mechanical instability and stacking of supports, and negative influence of dispersants. This study reveals that the 3D-KSC/NCNTs nanocomposites have great potential for various fields, such as fuel cells, sensing platforms and supercapacitors.

■ ASSOCIATED CONTENT

● Supporting Information

The Supporting Information is available free of charge on the ACS Publications website at DOI: 10.1021/acs.analchem.xxxxx.

Schematic illustration of the fabrication of 3D-KSC/NCNTs electrode, SEM images of 3D-KSC/NCNTs, 3D-KSC/Ni NPs and 3D-KSC/NCNTs obtained at the growth time of 20 min, CVs and LSV of different electrodes, stability test of 3D-KSC/NCNTs nanocomposites in ORR, EIS for 3D-KSC/NCNTs/GOD and 3D-KSC/GOD, stability and reproducibility of 3D-KSC/NCNTs/GOD biosensor, selectivity test of 3D-KSC/NCNTs/GOD biosensor, stability of sensor in the determination of human serum samples, comparison of the performance of various GOD-based glucose sensors and determination of glucose in blood serum sample. (PDF)

AUTHOR INFORMATION

Corresponding Author

*Tel/Fax: +86-791-88120861. E- mail: lwangsy2003@hotmail.com (L. Wang).

Notes

The authors declare no competing financial interest.

ACKNOWLEDGMENT

This work was financially supported by National Natural Science Foundation of China (21165010, 21465014 and 21465015), Natural Science Foundation of Jiangxi Province (20142BAB203101), Young Scientist Foundation of Jiangxi Province (20122BCB23011), The Ministry of Education by the Specialized Research Fund for the Doctoral Program of Higher Education (20133604110002) and the Ground Plan of Science and Technology Projects of Jiangxi Educational Committee (KJLD14023).

■ REFERENCE

(1) Luo, X.; Killard, A. J.; Smyth, M. R. *Electroanalysis* **2006**, *18*, 1131-1134.

(2) Cui, H. F.; Ye, J. S.; Zhang, W. D.; Sheu, F. S. *Biosens. Bioelectron.* **2009**, *24*, 1723-1729.

(3) Deng, C.; Chen, J.; Nie, Z.; Si, S. *Biosens. Bioelectron.* **2010**, *26*, 213-219.

(4) Cui, H. F.; Zhang, K.; Zhang, Y. F.; Sun, Y. L.; Wang, J.; Zhang, W. D.; Luong, J. H. *Biosens. Bioelectron.* **2013**, *46*, 113-118.

(5) Zhou, C.; Liu, J. *Nanotechnology* **2014**, *25*, 035402.

(6) Kong, L.; Yin, X.; Yuan, X.; Zhang, Y.; Liu, X.; Cheng, L.; Zhang, L. *Carbon* **2014**, *73*, 185-193.

(7) Chen, M.; Zhang, L.; Duan, S.; Jing, S.; Jiang, H.; Li, C. *Adv. Funct. Mater.* **2014**, *24*, 7548-7556.

(8) Yue, X.; Pang, S.; Han, P.; Zhang, C.; Wang, J.; Zhang, L. *Electrochem. Commun.* **2013**, *34*, 356-359.

(9) Lee, K. K.; Loh, P. Y.; Sow, C. H.; Chin, W. S. *Electrochem. Commun.* **2012**, *20*, 128-132.

(10) Noh, H.-B.; Lee, K.-S.; Chandra, P.; Won, M.-S.; Shim, Y.-B. *Electrochim. Acta* **2012**, *61*, 36-43.

(11) Guo, M. Q.; Hong, H. S.; Tang, X. N.; Fang, H. D.; Xu, X. H. *Electrochim. Acta* **2012**, *63*, 1-8.

(12) Song, M. J.; Hwang, S. W.; Whang, D. *Talanta* **2010**, *80*, 1648-1652.

(13) Li, C.; Su, Y.; Zhang, S.; Lv, X.; Xia, H.; Wang, Y. *Biosens. Bioelectron.* **2010**, *26*, 903-907.

(14) Wang, G.; Lu, X.; Zhai, T.; Ling, Y.; Wang, H.; Tong, Y.; Li, Y. *Nanoscale* **2012**, *4*, 3123-3127.

(15) Wang, L.; Zhang, Q.; Chen, S.; Xu, F.; Chen, S.; Jia, J.; Tan, H.; Hou, H.; Song, Y. *Anal. Chem.* **2014**, *86*, 1414-1421.

(16) Guo, Q.; Zhao, D.; Liu, S.; Chen, S.; Hanif, M.; Hou, H. *Electrochim. Acta* **2014**, *138*,

318-324.

(17) Guo, Y.; Guo, S.; Ren, J.; Zhai, Y.; Dong, S.; Wang, E. *ACS Nano* **2010**, *4*, 4001-4010.

(18) Wang, S.; Zhang, L.; Xia, Z.; Roy, A.; Chang, D. W.; Baek, J. B.; Dai, L. *Angew. Chem.* **2012**, *51*, 4209-4212.

(19) Wang, H.; Hao, Q.; Yang, X.; Lu, L.; Wang, X. *Nanoscale* **2010**, *2*, 2164-2170.

(20) Xu, J.; Wang, K.; Zu, S. Z.; Han, B. H.; Wei, Z. *ACS Nano* **2010**, *4*, 5019-5026.

(21) Chen, T.; Cai, Z.; Yang, Z.; Li, L.; Sun, X.; Huang, T.; Yu, A.; Kia, H. G.; Peng, H. *Adv. Mater.* **2011**, *23*, 4620-4625.

(22) Wei, W.; Liang, H.; Parvez, K.; Zhuang, X.; Feng, X.; Mullen, K. *Angew. Chem.* **2014**, *53*, 1570-1574.

(23) Shen, A.; Zou, Y.; Wang, Q.; Dryfe, R.; Huang, X.; Dou, S.; Dai, L.; Wang, S. *Angew. Chem., Int. Ed.* **2014**, *53*, 10804-10808.

(24) Yan, J.; Meng, H.; Xie, F.; Yuan, X.; Yu, W.; Lin, W.; Ouyang, W.; Yuan, D. *J. Power Sources* **2014**, *245*, 772-778.

(25) Liu, Q.; Pu, Z.; Tang, C.; Asiri, A. M.; Qusti, A. H.; Al-Youbi, A. O.; Sun, X. *Electrochem. Commun.* **2013**, *36*, 57-61.

(26) Xu, X.; Yuan, T.; Zhou, Y.; Li, Y.; Lu, J.; Tian, X.; Wang, D.; Wang, J. *Int. J. Hydrogen Energy* **2014**, *39*, 16043-16052.

(27) Wang, L.; Zheng, Y.; Wang, X.; Chen, S.; Xu, F.; Zuo, L.; Wu, J.; Sun, L.; Li, Z.; Hou, H.; Song, Y. *ACS Appl. Mater. Interfaces* **2014**, *6*, 7117-7125.

(28) Liu, R.; Wu, D.; Feng, X.; Mullen, K. *Angew. Chem.* **2010**, *49*, 2565-2569.

(29) Liu, Z. W.; Peng, F.; Wang, H. J.; Yu, H.; Zheng, W. X.; Yang, J. *Angew. Chem.* **2011**, *50*, 3257-3261.

(30) Wu, J.; Zhang, D.; Wang, Y.; Hou, B. *J. Power Sources* **2013**, *227*, 185-190.

(31) Bo, X.; Han, C.; Zhang, Y.; Guo, L. *ACS Appl. Mater. Interfaces* **2014**, *6*, 3023-3030.

(32) Tian, J.; Liu, Q.; Ge, C.; Xing, Z.; Asiri, A. M.; Al-Youbi, A. O.; Sun, X. *Nanoscale* **2013**, *5*, 8921-8924.

(33) Zhang, Y.; Chang, G.; Liu, S.; Lu, W.; Tian, J.; Sun, X. *Biosens. Bioelectron.* **2011**, *28*, 344-348.

(34) Lu, W.; Luo, Y.; Chang, G.; Sun, X. *Biosens. Bioelectron.* **2011**, *26*, 4791-4797.

(35) Periasamy, A. P.; Chang, Y. J.; Chen, S. M. *Bioelectrochemistry* **2011**, *80*, 114-120.

(36) Song, Y.; Liu, H.; Wang, Y.; Wang, L. *Electrochim. Acta* **2013**, *93*, 17-24.

(37) Mani, V.; Devadas, B.; Chen, S. M. *Biosens. Bioelectron.* **2013**, *41*, 309-315.

(38) Dai, Z.; Bao, J.; Yang, X.; Ju, H. *Biosens. Bioelectron.* **2008**, *23*, 1070-1076.

(39) Yang, C.; Xu, C.; Wang, X. *Langmuir* **2012**, *28*, 4580-4585.

(40) Wang, Y.; Liu, L.; Li, M.; Xu, S.; Gao, F. *Biosens. Bioelectron.* **2011**, *30*, 107-111.

(41) Laviron, E. *J. Electroanal. Chem.* **1979**, *101*, 19-28.

(42) Yao, Y. L.; Shiu, K. K. *Electroanalysis* **2008**, *20*, 1542-1548.

(43) Wu, P.; He, Y.; Wang, H. F.; Yan, X. P. *Anal. Chem.* **2010**, *82*, 1427-1433.

(44) Lad, U.; Kale, G. M.; Bryaskova, R. *Anal. Chem.* **2013**, *85*, 6349-6355.

FIGURE CAPTIONS

Scheme 1. Schematic illustration for the preparation of 3D-KSC/NCNTs nanocomposites.

Figure 1. SEM images of a piece of 3D-KSC: (A) overview (inset 1 and 2 show optical photograph of a piece of KS and 3D-KSC, respectively), (B) top view and (D) side view. SEM images of a piece of 3D-KSC/NCNTs: (C) top view, (E) side view and (F) cross-section view. Insets in Figure E and F show high magnification images.

Figure 2. (A) FT-IR spectroscopy and (B) N_2 adsorption/desorption isotherms for the 3D-KSC (black line) and 3D-KSC/NCNTs (red line). (C) Raman spectroscopy and (D) XPS spectra of the 3D-KSC/NCNTs (red line) and 3D-KSC (black line). Inset shows the high-resolution XPS spectrum for N 1s.

Figure 3. (A) CVs of 3D-KSC (black line) and 3D-KSC/NCNTs (red line) in air-saturated 0.1 M KOH solution with a scan rate of 100 mV s^{-1}. (B) CVs of 3D-KSC/NCNTs under different oxygen partial pressures. (C) Linear sweep voltammograms of 3D-KSC/NCNTs in O_2-saturated 0.1 M KOH solution with different rotation rates. (D) Koutecky−Levich plots of 3D-KSC/NCNTs at different electrode potentials. Inset: the dependence of electron transfer number *n* on potential for 3D-KSC/NCNTs.

Figure 4. (A) CVs of 3D-KSC/GOD (red line) and 3D-KSC/NCNTs/GOD (black line) in 0.2 M N_2-saturated PBS (pH 7.0) at a scan rate of 100 mV s^{-1}. (B) CVs of 3D-KSC/NCNTs/GOD in 0.2 M N_2-saturated PBS at different pH at a scan rate of 100 mV s^{-1} and inset: plots of E^0 versus pH. (C) CVs of 3D-KSC/NCNTs/GOD in 0.2 M N_2-saturated PBS at various scan rates from 100 to 1000 mV s^{-1} and inset: plot of peak current versus scan rates. (D) CVs of the 3D-KSC/NCNTs/GOD in 0.2 M O_2-saturated PBS (pH 7.0) at scan rate of 100 mV s^{-1} with glucose from 0, 2, and up to 22.0 mM. Inset shows the calibration curve at −0.40 V of 3D-KSC/NCNTs/GOD electrode.

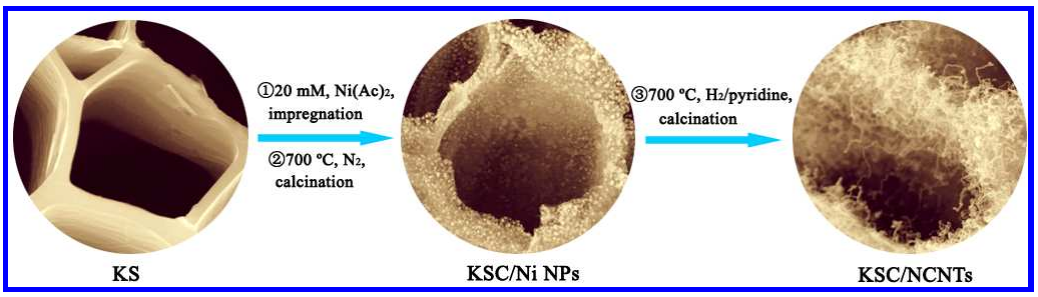
①20 mM, Ni(Ac)2, impregnation
②700 °C, N2, calcination
③700 °C, H2/pyridine, calcination
KS
KSC/Ni NPs
KSC/NCNTs

Scheme 1

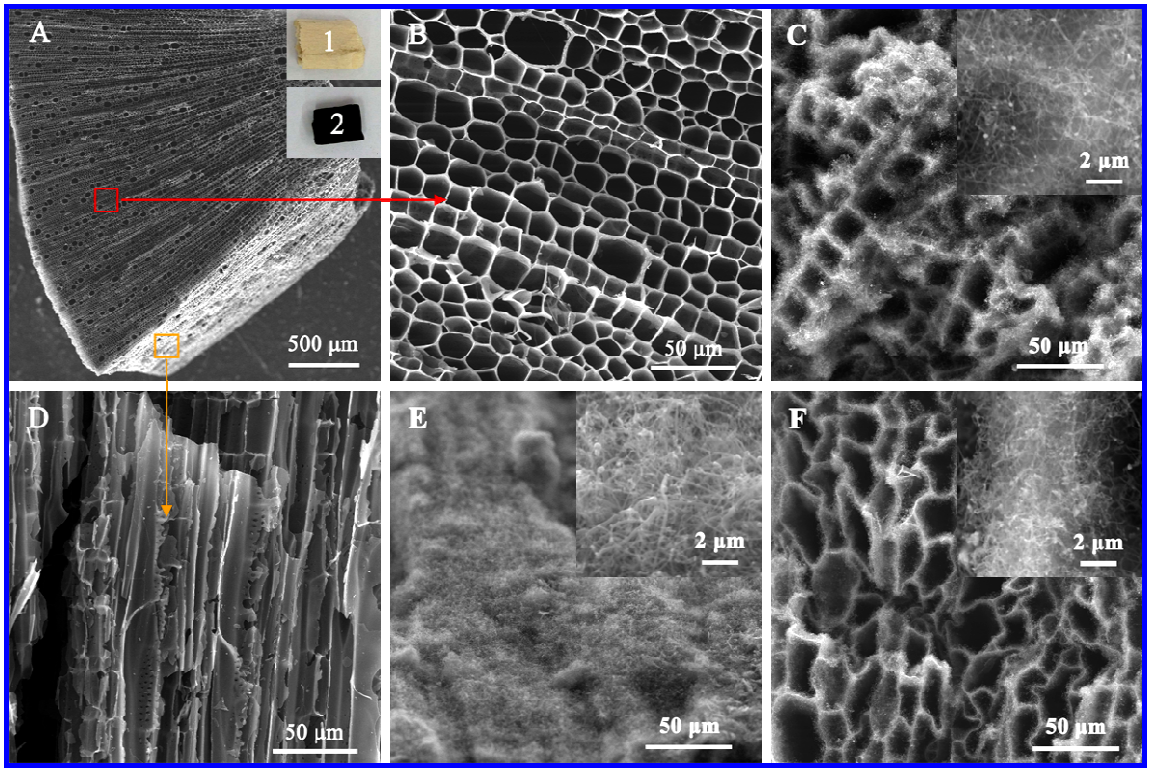

Figure 1

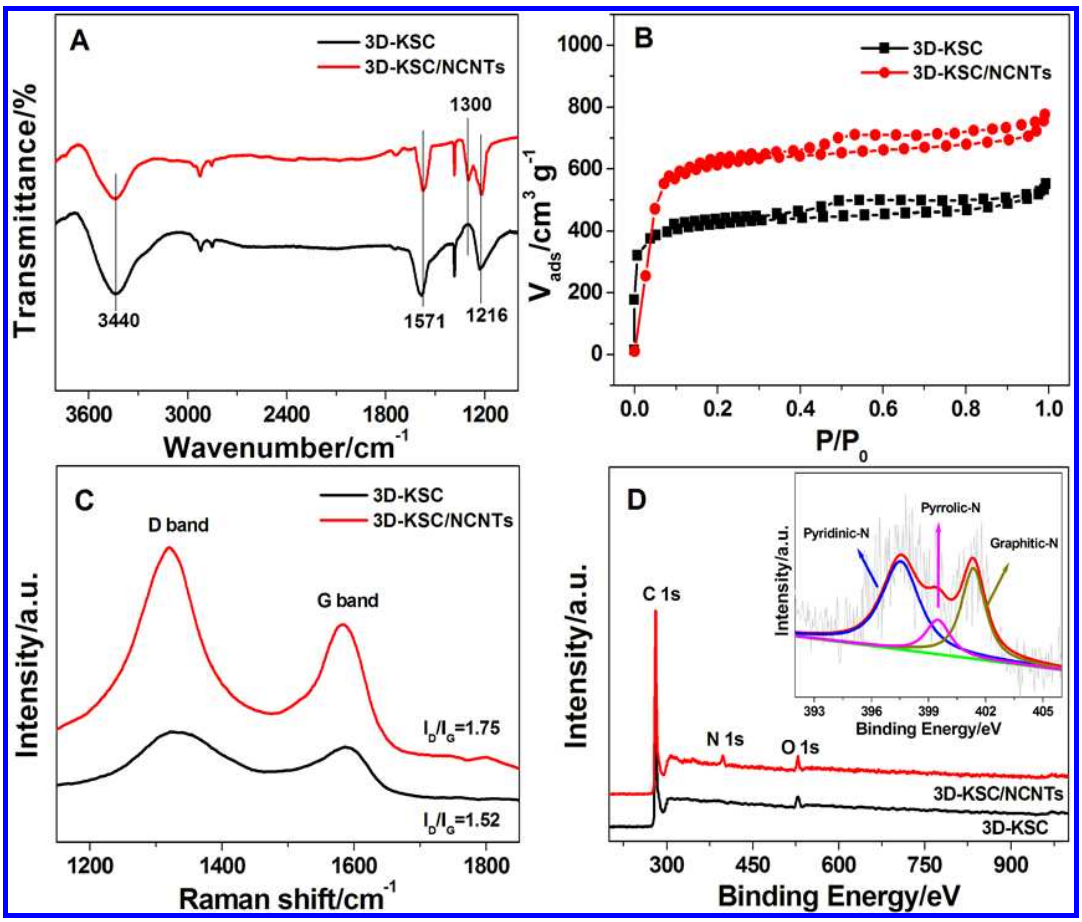
A
3D-KSC
3D-KSC/NCNTs
Transmittance/%
1300
3440
1571
1216
3600
3000
2400
1800
1200
Wavenumber/cm-1
B
3D-KSC
3D-KSC/NCNTs
Vads/cm3 g-1
1000
800
600
400
200
0
0.0
0.2
0.4
0.6
0.8
1.0
P/P0
C
3D-KSC
3D-KSC/NCNTs
D band
G band
Intensity/a.u.
ID/IG=1.75
ID/IG=1.52
1200
1400
1600
1800
Raman shift/cm-1
D
Intensity/a.u.
C 1s
N 1s
O 1s
Pyridinic-N
Pyrrolic-N
Graphitic-N
393
396
399
402
405
Binding Energy/eV
3D-KSC/NCNTs
3D-KSC
300
450
600
750
900
Binding Energy/eV

Figure 2

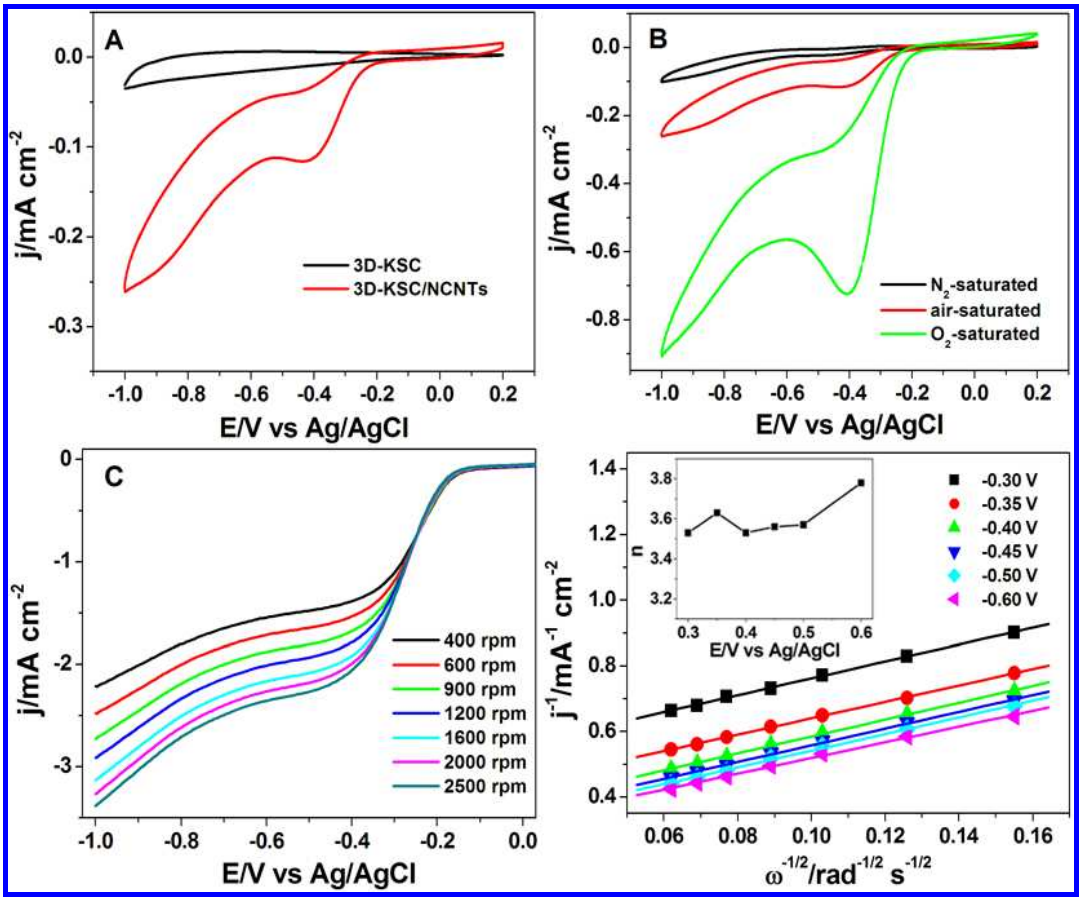
A
j/mA cm-2
E/V vs Ag/AgCl
3D-KSC
3D-KSC/NCNTs
B
j/mA cm-2
E/V vs Ag/AgCl
N2-saturated
air-saturated
O2-saturated
C
j/mA cm-2
E/V vs Ag/AgCl
400 rpm
600 rpm
900 rpm
1200 rpm
1600 rpm
2000 rpm
2500 rpm
j-1/mA-1 cm-2
ω-1/2/rad-1/2 s-1/2
n
E/V vs Ag/AgCl
-0.30 V
-0.35 V
-0.40 V
-0.45 V
-0.50 V
-0.60 V

Figure 3

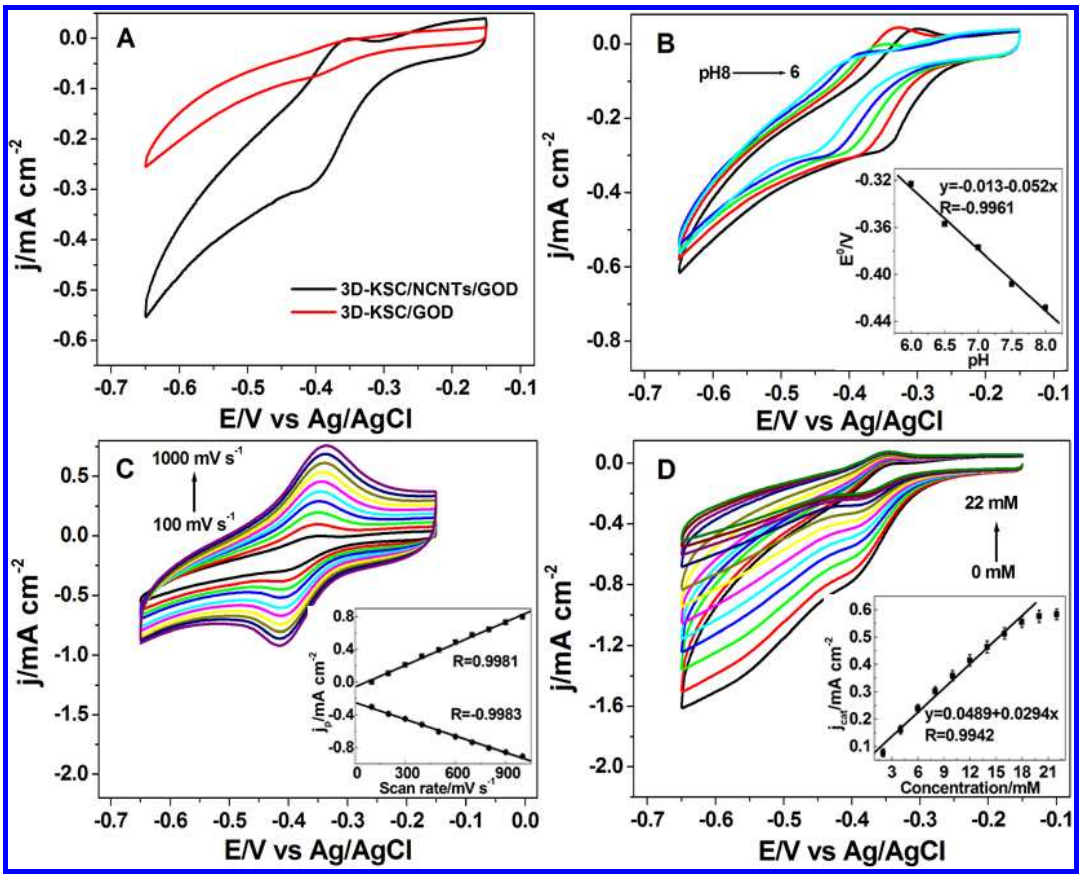
A
3D-KSC/NCNTs/GOD
3D-KSC/GOD
j/mA cm-2
E/V vs Ag/AgCl
B
pH8 → 6
y=-0.013-0.052x
R=-0.9961
E°/V
pH
C
1000 mV s-1
100 mV s-1
R=0.9981
R=-0.9983
Scan rate/mV s-1
D
22 mM
0 mM
y=0.0489+0.0294x
R=0.9942
Concentration/mM

Figure 4

TOC

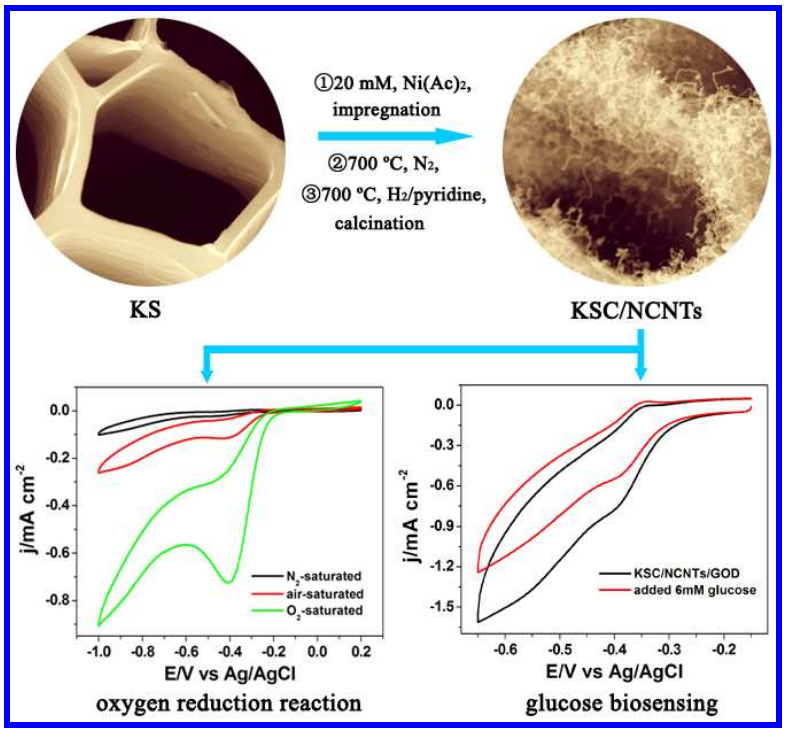

For Table of Contents only